Geophysical Journal International

Geophys. J. Int. (2013) **193,** 329–337 doi: 10.1093/gji/ggs107

Moho structure of the Anatolian Plate from receiver function analysis

E.A. Vanacore,[1,*] T. Taymaz[2] and E. Saygin[1]

[1] *The Australian National University, Research School of Earth Sciences, Canberra, Australia. E-mail: E.Vanacore@leeds.ac.uk*
[2] *Istanbul Technical University, The Faculty of Mines, Department of Geophysical Engineering, Maslak* 34469*, Istanbul, Turkey*

Accepted 2012 December 11. Received 2012 October 22; in original form 2012 March 09

SUMMARY

Here we present first-order results detailing the Anatolian crustal from receiver function analysis of data from approximately 300 stations within Turkey. Seismic data from the Kandilli Observatory array (KOERI; KO), the National Seismic Network of Turkey (AFAD-DAD; TU) and available IRIS data from the Northern Anatolian Fault experiment (YL) for the period between 2005 and 2010 is analysed. We calculate receiver functions in the frequency domain using water-level deconvolution. The results are analysed using a combination of H–K stacking and depth stacking to determine robust Moho conversion depths and V_P/V_s ratios across Anatolia. We detect a deep Moho in eastern Anatolia of up to ∼55 km, a generally normal Moho in Central Anatolia of ∼37–47 km and a thinned Moho in western Anatolia and Cyprus of ∼30 km. The V_P/V_s ratio across the Anatolian Plate is generally slightly elevated; regions of extremely high V_P/V_s ratio (>1.85) can be associated with recent volcanism in eastern and central Anatolia. High V_P/V_s ratio measurements (>1.85) in western Anatolia may be indicative of partial melt in the lower crust associated with regional extension.

Key words: Body Waves; Crustal Structure; Europe.

INTRODUCTION

Anatolia is a complex amalgamation of multiple tectonic regimes controlled by the interaction of the Arabian, African and Anatolia plates. Estimates of regional deformation and major fault movements from GPS measurements divide the area covered in this study into a few major geodynamic regions including the N–S extensional region in western Turkey, a region of strike-slip extension in the northwest, the stable central interior with <2 mm yr^{-1} of internal deformation that is bound by the North Anatolian and East Anatolian fault (EAF) and a region of distributed strike-slip deformation in eastern Turkey (Taymaz *et al.* 1991a,b; McClusky *et al.* 2000; Şengör *et al.* 2005; Tan & Taymaz 2006; Fig. 1). Past seismic studies have concentrated on single aspects of these neotectonics by examining crustal structure on regional scale lengths (e.g. Saunders *et al.* 1998; Karabulut *et al.* 2003; Zor *et al.* 2003; Lei & Zhao 2007; Özacar *et al.* 2010; Salah *et al.* 2011). In this study, we use the large scale coverage of the Anatolian Plate available from the Kandilli Observatory Seismic Array (KOERI; KO), the National Seismic Array of Turkey (AFAD-DAD) and the Northern Anatolian Fault Experiment of IRIS Passcal Expedition to generate plate scale Moho depth structure and V_P/V_s ratio maps of the Anatolian Plate.

DATA AND METHODS

We use teleseismic events with a magnitude range of $5.5 \leq M_w \leq 7.0$ recorded on the three-component instruments available from the Kandilli Observatory array (KO), the National Seismic Network of Turkey (TU) and the Northern Anatolian Fault Experiment (YL) during the period between 2005 and the middle of 2010 (Fig. 1). Given the time period of the data and the large number of stations available for analysis, ∼300, there is an abundance of stations with good epicentral distance and azimuthal coverage despite a slight azimuthal bias to events in the northeastern quadrant (Fig. 2c). Receiver function analysis (Burdick & Langston 1977; Owens *et al.* 1984) exploits the *P* to *S* converted phases arriving just after the direct *P* arrival to determine crustal structure. There exist a variety of receiver function techniques that employ either a time or frequency domain deconvolution to retrieve signals related to crustal structure (e.g. Ammon 1991; Gurrola *et al.* 1994; Ligorria & Ammon 1999; Park & Levin 2000; Poppeliers & Pavlis 2003; Helffrich 2006). In this study, we select events with a signal-to-noise ratio (SNR) of at least two and rotate to the radial, transverse and vertical coordinate system (RTZ) before performing a frequency domain water-level deconvolution (Clayton & Wiggins 1976; Ammon 1991). We calculate receiver functions with a cut off frequency of 1 Hz and a water level of 0.03 for a time period between 20 s before *P* to 100 s after *P*. To ensure further stability of the deconvolution process and results, we additionally generate and process a set of receiver functions using a higher water level of 0.2. Resulting Moho depth

[*] Now at: University of Leeds, School of Earth and Environment, Leeds, UK.

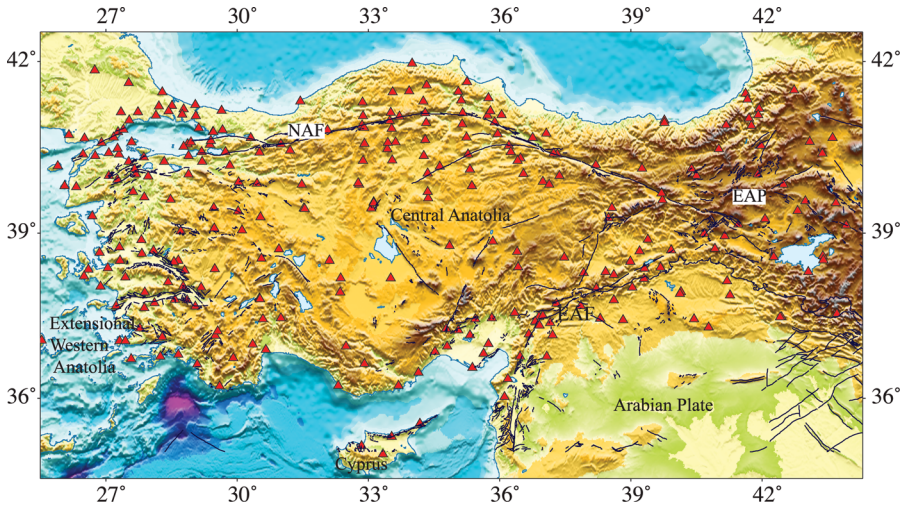

Figure 1. Distribution of temporary and permanent seismic stations analysed in this study (red triangles). Black lines denote the known faulting after Taymaz *et al.* (2004). Major structures and regions discussed in this paper are labelled as the Extensional western Anatolia characterized with numerous extensional fault zones, the stable central Anatolian interior, the island of Cyprus, the East Anatolian Fault (EAF), the North Anatolian Fault (NAF) and the Eastern Anatolian Plateau (EAP).

measurements were generally consistent between the two different receiver function sets indicating a stable deconvolution at the lower water level. However, data from the YL array do not appear stable at the lower water level, so the higher water level of 0.2 was used in the analysis. We focus on the first 40 s after *P* to isolate crustal structure information within the receiver functions; the longer time period was used so that the computed receiver functions can be used in future investigations of mantle transition zone structure. The final receiver functions used in further analysis were required to pass a further SNR filter (SNR $>$ 2) based on the initial peak as well as a visual inspection to ensure only stable receiver functions were used in the final product. The number of useable receiver functions used after ensuring a good recovery of the data for each station varies from the order of tens to hundreds (See supplemental data table for details.). Fig. 2 shows an example of the typical receiver functions both radial and transverse, labelled R and T respectively, generated by the process described above for the Kandilli array station LOD (39.89°N, 32.76°E). The linearly stacked receiver functions (Fig. 2a) show a clear *P* to *S* Moho conversion at approximately 4.5 s after the first arrival. In the case of this particular station, the crustal multiples such as the 2p1s, referring to two *P*-wave and one *S*-wave legs in the crust, are significantly weaker. The 2p1s multiple is faintly visible in binned ray parameter plots at approximately 8 s (Fig. 2b) but not clearly visible in the 5-deg binned backazimuthal sweep (Fig. 2c).

To derive first-order measurements of the depth to the Moho beneath each individual station, we perform the modified Zhu & Kanamori (2000) H–K stacking method of Niu & James (2002) to the receiver functions for each station. We assume a crustal velocity of 6.2 km s^{-1} and use a V_P/V_s ratio of 1.5–2.0 with a 0.005 sampling and Moho depth range of and 20–60 km with a 1 km sampling. The H–K stacking technique does fail in some rare occurrences such as the presence of a dipping Moho, gradational Moho structure, or the presence of a strong mid-crustal structure (Ammon *et al.* 1990; Cassidy 1992). We therefore take a couple of extra processing steps in our analysis. First, for each station we perform a depth stacking for the direct *P* to *S* conversion based on the IASP91 velocity model (Kennett & Engdahl 1991), which assumes a V_P/V_s ratio of approximately 1.73 to determine an 'idealized' depth of the Moho. In complex environments such as our study area, the V_P/V_s ratio can be far removed from the assumed 1-D model and multiple maxima from structure may be present. We therefore only look for consistency with the depth stack if the resultant H–K V_P/V_s ratio is near 1.73 and appears to have a simple structure in the azimuth and slowness sweeps. Second, we vary the weighting factor of the receiver function multiples in the H–K stacking process. We calculate two sets of H–K stacks where the first set has the following weighting: 0.5 for the *P*s, 0.25 for the 2p1s multiple and 0.25 for the 1p2s multiple. The second stack is given no weight to the consistently weaker 2s1p multiple in our data set such that the weight is 0.5 for the *P*s phase, 0.5 for the 2p1s multiple and 0.0 for the 1p2s multiple. A consistent Moho depth measurement and V_P/V_s ratio across the different H–K stacks is considered an ideal result. An example of such a result from the station LOD is shown in Fig. 3. Figs 3(a)–(c) shows three H–K stacks showing the results from different weighting of the multiples (Figs 3a–b) and a different water-level value, *k*, (Fig. 3c) during processing. Fig. 3(d) shows the family of models generated by the depth stacking combined a bootstrap resampling process where each stack contains a 70 per cent sample of the data (Efron & Tibshirani 1986). Both the H–K stacking and depth stacking techniques produce well-defined Moho data point. Note that in this particular case the H–K stack and depth stack determination of Moho depths are in good agreement because the V_P/V_s ratio determined by the H–K method is close to the 1.73 V_P/V_s ratio of the IASP91 model (Kennett & Engdahl 1991). The stacking case shown in Fig. 3 is considered an ideal result given that all four stacks show a consistent depth and V_P/V_s ratio. In extreme cases where the Moho in the H–K stack does not produce a quality result, such as when the stacking process produces a curve of probable depth and ratio values, we do not include an estimation of the Moho depth or V_P/V_s ratio in the map.

Previous receiver functions studies show the presence of dipping structures and anisotropy affect the amplitude ratio of the *P* and *P*s phases between transverse and radial receiver functions and cause waveform variation along backazimuth (e.g. Peng & Humphreys 1997; Savage 1998). Given that Anatolia is a complex tectonic environment, we expect that anisotropic effects will be visible in our data. We identify anisotropy that is visible in the *P*s phase

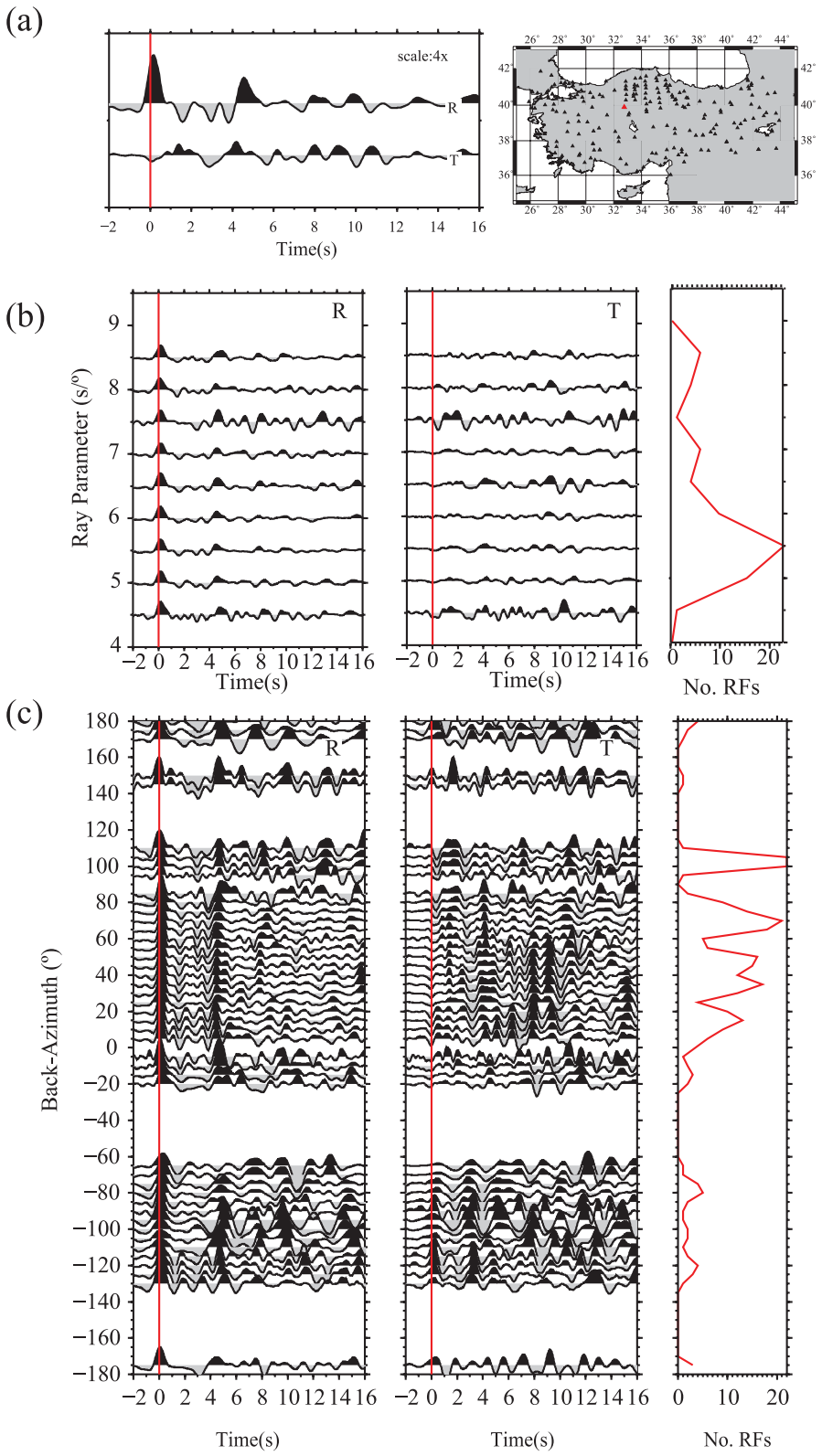

Figure 2. Characteristic results of the receiver function study for the station LOD (39.89°N, 32.76°E). (a) Linearly stacked results for all used receiver functions for both the radial (R) and transverse components (T). (b) 0.5 s/° binned stacks of the receiver functions for the radial (right) and transverse (middle) receiver functions based on ray parameter. The number of receiver functions per bin is shown in the third column. (c) Same as part b but binned by backazimuth rather than ray parameter.

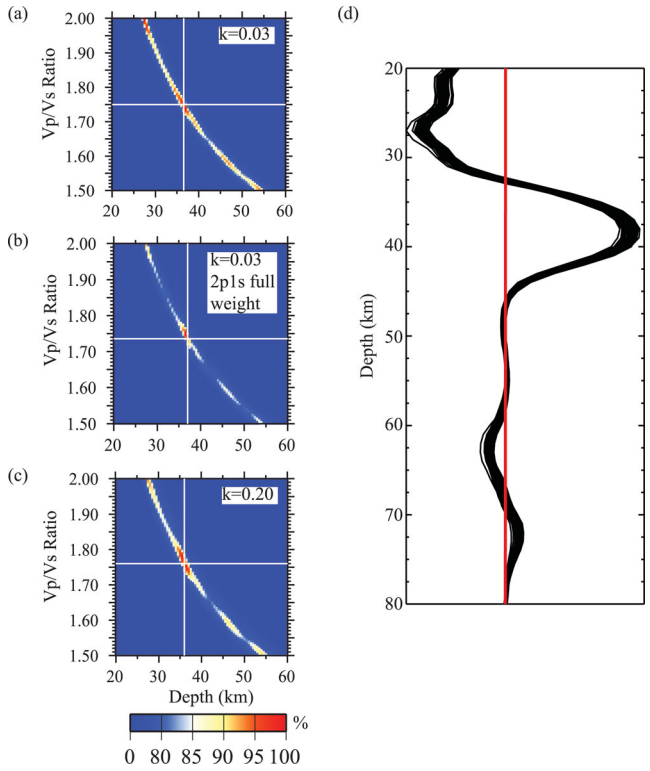

Figure 3. Example of the H–K and depth stacking analysis for the station LOD (39.89⟨°⟩N, 32.76⟨°⟩E). (a) H–K stack with equal weight on the peg-leg multiples for receiver functions calculated using a water-level, k, equal to 0.03. (b) The same as part (a) but with all weight on the 2p1s multiple and 0 weight on the 1p2s multiple. (c) The same as part (a) but for radial receiver functions calculated with a water level of 0.2. (d) Depth stacking results showing the energy calculated for *P* to *S* conversions at a given depth. Each line shows one result of the bootstrap resampled data for 100 iterations and a 70 per cent sample rate of the data. Note that family of results indicate a Moho conversion at ∼38 km depth which is similar to the results from the H–K stacking results because of the similar V_P/V_s ratios in this example.

backazimuth sections of the transverse receiver functions and identify possible dipping structures by calculating the average transverse to radial amplitude of the *P* wave (e.g. Savage 1998). Stations with such characteristics are identified in the supplementary data table and omitted from the final plot if deemed to have an unacceptable level complexity. The majority of stations with either the backazimuth variation of the *P*s or a high ratio are located either along the western and southern coastlines or within the Eastern Anatolian Plateau (See supplemental data table). This is consistent with studies that have identified similar response beneath regions other complicated regions such as the Tien Shan (e.g. Vinnik *et al.* 2007).

The primary product of this project is large-scale maps of Moho depth and V_P/V_s ratio across the entire Anatolian Plate (Fig. 4). To generate the maps we first incorporate receiver function results from previous regional studies where the numerical values of Moho depth and/or V_P/V_s ratio are readily available (Saunders *et al.* 1998; Özacar *et al.* 2010; Yolsal-Çevikbilen *et al.* 2012) with the results from the analysis preformed in this study. We then use routine of Smith & Wessel (1990) available in the generic mapping tools to grid and create a surface reflecting Moho depth with a tension value of 0.45 after running the data through a routine determining the median value of each 0.5 × 0.5 degree square. We further mask the portions of the resulting surface that are further than 75 km away from individual station locations to avoid attributing either a Moho depth or V_P/V_s ratio to an undersampled portion of the overall plate. The resultant maps (Fig. 4) provide a smoothed image of Anatolian crustal for interpretation of large-scale features of the plate.

RESULTS AND DISCUSSION

For the purposes of this discussion we focus upon the large wavelength features across Anatolia. Details of small-scale features are highlighted by the individual stations symbols in Fig. 4; these regional scale features have been discussed extensively by focused studies (e.g. Saunders *et al.* 1998; Zor *et al.* 2003; Özacar *et al.* 2010; Yolsal-Çevikbilen *et al.* 2012). The most distinct large scales feature of the Anatolian Plate is the gradient from a thinner crust in the extensional West to a 'normal' crustal thickness in central Anatolia to a thickened crust in the compressional regime in eastern Anatolia (Fig. 4a). The Eastern Anatolian Fault demarks a sharp change in Moho depth between ∼36°E and 38°E. To the North within the Anatolian Plate Moho depths are ∼40–45 km whereas to the South within the Arabian Plate Moho depth are ∼30–35 km. This change in crustal thickness is consistent with previous regional studies by Özacar *et al.* (2010) and Zor *et al.* (2003). The depth change may reflect a geological difference between the Arabian and Anatolian Plate, but the receiver functions in this study lack the spatial resolution necessary to definitively conclude that the EAF is the demarcation of the Anatolian–Arabian Plate boundary in this region.

The East Anatolian Plateau is a consequence of the current continent–continent collision with the Arabian Plate and is bounded by the North Anatolian Fault (NAF) and EAF, which subsequently demark the escape of the Anatolian Plate to the West (McKenzie 1978; Şengör & Yılmaz 1981; Taymaz *et al.* 1991a,b; Bozkurt 2001; Taymaz *et al.* 2004, 2007a,b; Yolsal-Çevikbilen & Taymaz 2012). Depths to the Moho of approximately 40–55 km dominate the Eastern Anatolian Plateau with the deepest Moho measurements tending to the North and Northeast. These measurements are consistent with a local high topography (∼2 km) being supported by mantle forces (e.g. Şengör *et al.* 2003) or slab break-off (e.g. Keskin 2003) rather than crustal thickening as previously suggested (Dewey *et al.* 1986). Anomalously high V_P/V_s ratios, >1.9, in northeastern Anatolia have previously been reported and attributed to volcanic activity in the region and partial melt in the crust (Özacar *et al.* 2010; Salah *et al.* 2011). Similarly, results from this study indicate high V_P/V_s ratios in eastern Anatolia that can be primarily associated with geologically recent volcanic activity.

The stable central Anatolian block is the least constrained region due the scarcity of seismic stations deployed in the region. Although the Moho depth measurements are variable across the block with Moho depth values varying from approximately 31 to 45 km as one would expect over a broad region, the median value of the depth to the Moho is approximately 37 km; this value is consistent with typical continental crustal thicknesses. The block is characterized by elevated V_P/V_s ratio with the exception of an anomalously high V_P/V_s ratio of ∼1.9 along a major splay of the NAF (Fig. 4b). The exceptionally high V_P/V_s ratio along the splay fault also as with high ratios in eastern Anatolia is associated with a region of middle Eocene volcanism (e.g. Yilmaz 1990; Keskin *et al.* 2008). The tectonic mechanism controlling this magmatism however is not well determined; the proposed mechanisms vary from continental collision (Genç & Yılmaz 1997) to active continental margins (Okay & Satır 2006) to recent slab break-off models similar to those presented to explain volcanism and crustal structure in eastern Anatolia

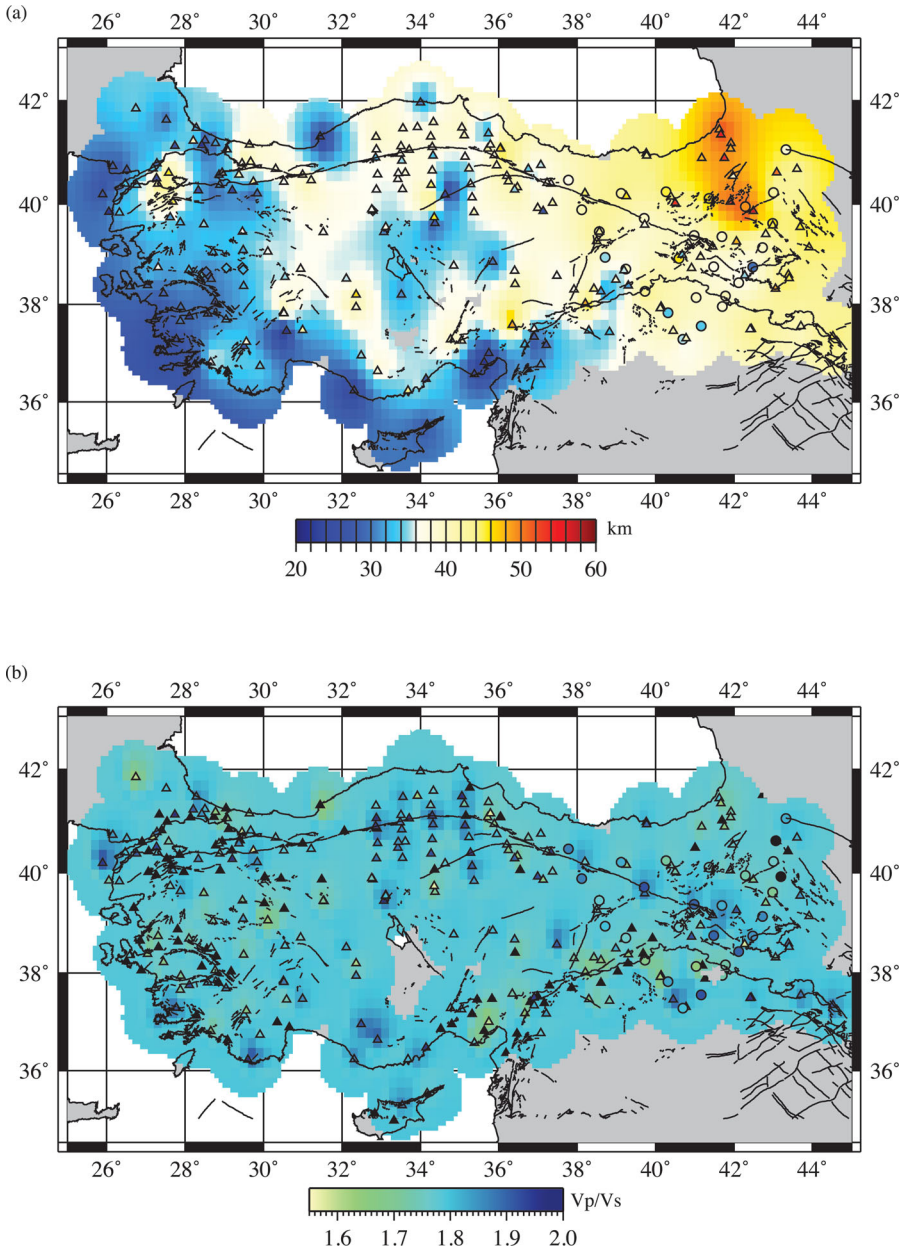

Figure 4. (a) Top: Moho map of Turkey for the current receiver function data set for stations with a minimum of five receiver functions. In addition to data from this study legacy data from Özacar *et al.* (2010) and Saunders *et al.* (1998) have been included in the mapping process. The Moho is generally deeper in the East and Northeast and thins to the South and West across Anatolia. (b) Bottom: The V_P/V_s ratio map shows a highly variable ratio throughout the region. To the first order, high V_P/V_s ratios appear to be roughly associated with tectonically active regions in the West and regions of recent (Eocene and later) volcanism in Central and eastern Turkey.

(e.g. Keskin 2003; Keskin *et al.* 2008). The Moho detected in this study where the V_P/V_s ratio is at its peak is not significantly thicker than predicted for a normal continental crust with variable depths detected between 37 and 45 km. This observation indicates that the continental collision model to explain the local volcanism is an unlikely candidate, as this model would result in a significantly thickened crust, which we do not observe. Our data does not provide sufficient information to differentiate between the active continental margin model (Okay & Satir 2006) and the slab break-off model (Keskin 2003; Keskin *et al.* 2008). The remaining slightly elevated V_P/V_s ratios of ∼1.8 in central Anatolia may be associated with the widely observed Neogene-Quaternary aged Central Anatolian Volcanic Province (CAPV) located south of the splay fault (e.g. Pasquarè *et al.* 1988; Yilmaz 1990). However, the sparse sampling available in this region prevents a conclusive delineation and determination of the size, shape, spread and association of this zone with the CAPV.

Along the southern edge of central Anatolia and Cyprus between 34° and 36°E and South of 36°N the depth to Moho thins significantly to values of ∼30 km. These values are consistent with tomography results including the island that retrieved Moho depths of ∼27 to 31 km depth (Koulakov & Sobolev 2006). Although the majority of receiver functions in this study result in a consistent simple Moho depth result similar to that shown in Figs 2 and 3, there do exist in rare cases evidence for more complicated structures. Receiver functions calculated for the seismic station CSS

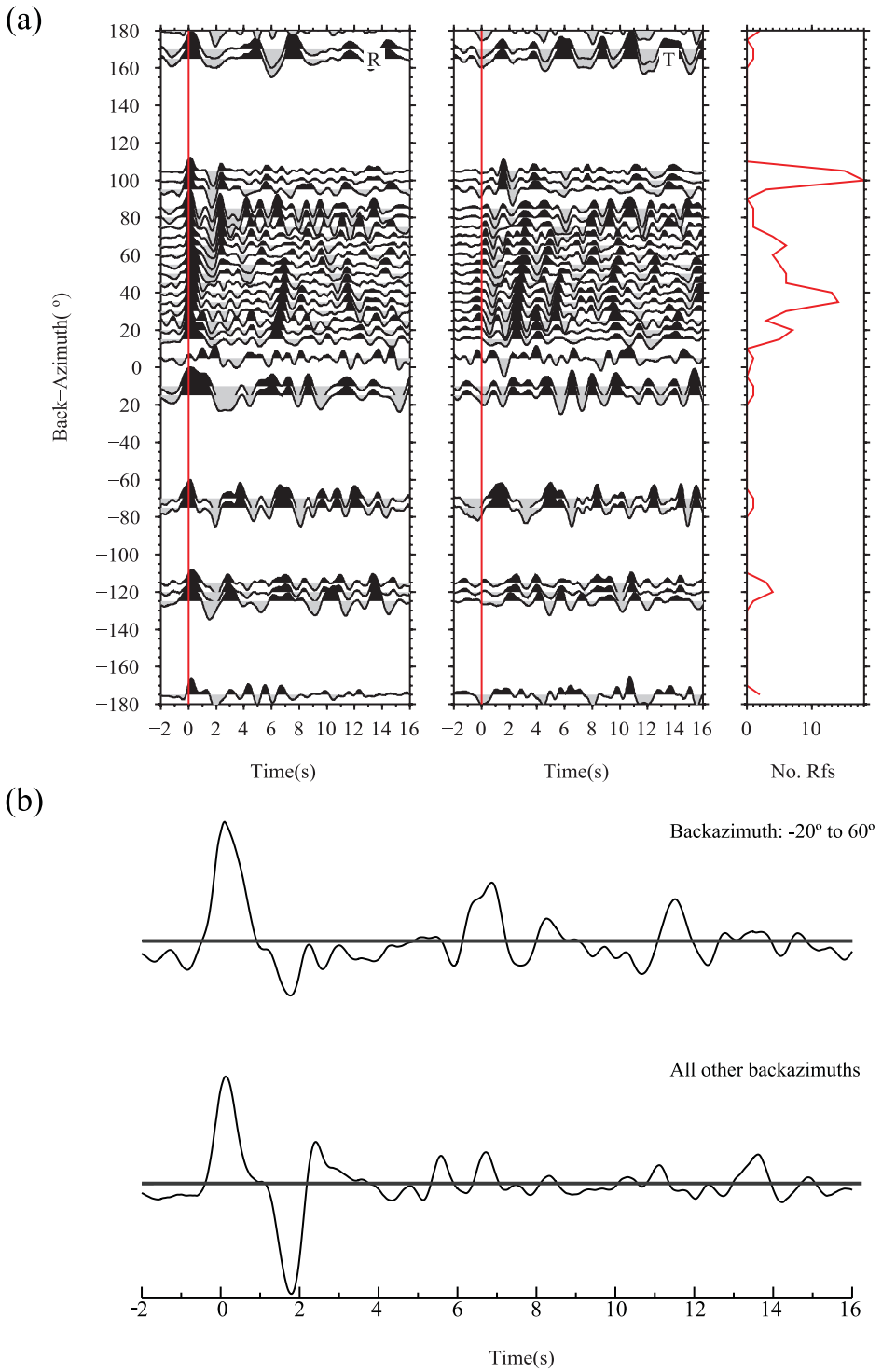

Figure 5. Receiver function results for the station CSS on Cyprus (33.33 ⟨°⟩ N, 34.96 ⟨°⟩ E). (a) Backazimuth sweeps for the radial (left) and transverse (middle) receiver functions and receiver function hit count (right) binned the same way as Fig. 2c. Note the highly variable *P* to *S* conversion across the sweep notably between 60 and −20° backazimuth where the signal is dominated by an arrival at about 7 s. (b) Stacked receiver functions for the anomalous zone (top) and the remaining receiver functions. The top receiver function is dominated by a signal at ∼7 s which corresponds to a conversion near 55 km depth. We interpret this signal as an indicator of the top of the Cyprean slab. The remaining receiver functions show a much earlier conversion near 3 s or ∼20 km depth; we interpret this as the Moho as it is in good agreement with other stations less than 50 km away.

located on Cyprus (33.33 ⟨°⟩ N, 34.96 ⟨°⟩ E) show a high dependence on the backazimuth (Fig. 5a). The receiver functions from sources with backazimuths between −20° and 60° appear consistent with a deep dipping structure whereas the remaining receiver functions have a *P* to *S* conversion visible approximately 3 s after the direct *P* wave (Fig. 5b). The former is consistent with a conversion depth of ∼55 km whereas the latter is consistent with an extremely shallow conversion of ∼21 km depth. The deeper detected conversion is concurrent with the approximate depth to the Cyprean slab beneath the island as determined by

previous seismicity and tomographic studies (Biryol *et al.* 2011; Kalyoncuoğlu *et al.* 2011). Given the variation with backazimuth and the two distinct regimes of the shallow and deep conversions our preferred interpretation is that the deep conversion at 55 km is a *P* to *S* converted phase from the subducted slab whereas the shallow conversion is because of local crustal structure. Observations of subducted slab structure have previously been made in studies along other margins such as the Pacific Northwest or South America (e.g. Audet *et al.* 2010; Gans *et al.* 2011) This type of observation is not unique in our data and occurs in multiple stations along the western and southern coasts of Anatolia. Stations where this phenomenon is present are reprocessed stacking data in azimuths that do not appear to have a significant component of slab interference and re-stacking the data with a reduced depth range 20–40 km to identify the probable Moho conversion. Data with this extra processing are labelled in the supplementary data table and should be used with the upmost caution.

Western Antatolia is characterized by N–S extension that results in the formation of graben structures and related E–W striking normal faulting (Taymaz *et al.* 1991a; Taymaz & Price 1992; Taymaz 1993; Jackson 1994). Consequently, western Anatolia is dominated by on average shallower Moho depth coupled with shorter wavelength variability compared to its eastern and central counterparts (Fig. 4a; Taymaz 1996). This variability is also observed in magnetotelluric studies in southwest Anatolia along 29°E between 37°N and 36°N where crustal thickness was shown to vary between ∼30 and 50 km (Gürer *et al.* 2004). The variability in Moho depths and elevated V_P/V_s ratio (Fig. 4) in this region is best explained by the current rapid extensional tectonics of southwest Anatolia (McClusky *et al.* 2000). The high V_P/V_s ratios coupled with observed high heat flow measurements in the regions provide further support to the conjecture that partial melt is present in the western Anatolian lower crust (Ercan *et al.* 1985; İlkışık 1995; Gürer *et al.* 2001). The variable Moho depth observations and V_P/V_s ratio observations are consistent with an extensional regime where thinned crust can be roughly associated with graben formation bound by normal faulting and thicker crust may be associated with areas of greater tectonic strength that have resisted the extensional forces (Fig. 4).

CONCLUSIONS

Here we presented the first plate scale Moho and V_P/V_s ratio map of the Anatolian Plate based on H–K stacking of receiver functions for approximately 300 stations using data spanning variable lengths with the period between 2005 and 2010. The depth to the Moho increases from west to east from less than 30 km to greater than 50 km beneath the Eastern Anatolian Plateau reflecting the transitions from extensional tectonics in the West to the stable central Anatolian Plate to the compressional tectonic regime in the east. The V_P/V_s ratio has a general tendency to be high across the plate (Yolsal-Çevikbilen *et al.* 2012), but the highest ratios are constrained in the east/central plate to regions of recent volcanism (Yilmaz 1990; Keskin *et al.* 2008). In the west the V_P/V_s ratios may indicate the presence of partial melt in the crust, which is consistent with the high heat flow and extensional graben structures present in the region (İlkişik 1995; Gürer *et al.* 2001).

The data and results in this study the first step in characterizing the large scale variations of crustal structure throughout the region. The shear volume of data available and the potentially complex structure of the region as exemplified by the seismic station CSS results brings its own set of challenges as well as opportunities. Here we presented 'long wavelength' results to provide a general picture of the Anatolian Plate structure; avenues for future studies will concentrate on determining the higher wavelength structure and individual station velocity structures. Because the stations in this study provide continuous data our long-term future goal is to combine the receiver function data calculated in this study with ambient noise information to generate a detailed view of the Anatolian crust.

ACKNOWLEDGMENTS

The authors would like to thank the Kandilli Observatory and Earthquake Research Institute (UDIM), the National Seismic Array of Turkey (AFAD-DAD) and IRIS for providing the data. We also thank Michelle Salmon for her useful advice in generating the large-scale maps. We are grateful to Yeşim Çubuk and Seda Yolsal-Çevikbilen for their efforts in gathering Turkish earthquake data. Figures in this paper were generated using the Generic Mapping Tools (GMT) developed by Smith and Wessel. This study was partially funded by Istanbul Technical University Research Fund (ITU-BAP), Turkish National Scientific and Technological Foundation (TUBITAK), Turkish Academy of Sciences (TUBA) in the framework for Young Scientist Award Program (TUBA–GEBIP 2001). Careful reviews by the two anonymous referees resulted in considerable improvement to an earlier version of this manuscript. We are particularly indebted to the Editor for his judicious insightful remarks.

REFERENCES

Ammon, C.J., Randall, G.E. & Zandt, G., 1990. On the non-uniqueness of RF inversions, *J. geophys. Res.,* **95,** 15 303–15 318.

Ammon, C.J., 1991. The isolation of receiver effects from teleseismic P waveforms, *Bull. seism. Soc. Am.,* **81,** 2504–2510.

Audet, P., Bostock, M.G., Boyarko, D.C., Brudzinski, M.R. & Allen, R.M., 2010. Slab morphology in the Cascadia fore arc and its relation to episodic tremor and slip, *J. geophys. Res.,* **115,** doi:10.1029/2008JB006053.

Biryol, C.B., Beck, S.L., Zandt, G. & Özacar, A.A., 2011. Segemented African lithosphere beneath the Anatolian region inferred from teleseismic P-wave tomography, *Geophys. J. Int.,* **184,** 1037–1057, doi:10.111/j.1365-246X.2010.04910.x.

Bozkurt, E., 2001. Neotectonics of Turkey: a synthesis, *Geodinamica Acta,* **14,** 3–30.

Burdick, L.J. & Langston, C.A., 1977. Modeling crustal structure with converted phases in teleseismic body-wave forms, *Bull. seism. Soc. Am.,* **67,** 677–691.

Cassidy, J.F., 1992. Numerical experiments in broadband receiver function analysis, *Bull. seism. Soc. Am.,* **82,** 1453–1474.

Clayton, R.W. & Wiggins, R.A., 1976. Source shape estimation and deconvolution of teleseismic body waves, *Geophys. J. R. astr. Soc.,* **47,** 151–177.

Dewey, J.F., Hempton, M.R., Kidd, W.S.F., Saroglu, F. & Sengör, A.M.C., 1986. Shortening of continental lithosphere: the neotectonics of Eastern Anatolia—a young collision zone, in *Collision Tectonics,* Vol. 19, (R. M. Shackleton volume), pp. 3–36, eds Coward, M.P. & Ries, A.C., Geol. Soc. London Spec. Pub.

Efron, B. & Tibshirani, R., 1986. Bootstrap methods for standard errors, confidence intervals, and other measures of statistical accuracy, *Stat. Sci.,* **1,** 54–75.

Ercan, T., Satır, M., Kreuzer, H., Turkecan, A., Günay, E., Çevikbaş, A., Ateş, M. & Can, B., 1985. Batı Anadolu Senozoyik volkanitlerine ait yeni kimyasal, izotropik ve radyometrik verilerin yorumu, *Bull. Geol. Soc. Turkey,* **28,** 121–136 (in Turkish).

Gans, C.R., Beck, S.L., Zandt, G., Gilbert, H., Alvarado, P., Anderson, M. & Linkimer, L., 2011. Continental and oceanic crustal structure of the Pampean flat slab region, western Argentina, using receiver function

analysis: new high-resolution results, *Geophys. J. Int.,* **186**(1), 45–58, doi:10.1111/j.1365-246X.2011.05023.x.

Genç, Ş.C. & Yılmaz, Y., 1997. An example of post-collisional magmatism in northwestern Anatolia: the Kızderbent volcanics (Armutlu peninsula, Turkey), *Turkish J. Earth Sci.,* **6,** 33–42.

Gürer, A., Gürer, Ö.F., Pinçe, A. & İlkışık, O.M., 2001. Conductivity Structure along the Gediz Graben, West Anatolia, Turkey: tectonic Implications, *Int. Geol. Rev.,* **43**(12), 1129–1144.

Gürer, A., Bayrak, M. & Gürer, Ö.F., 2004. Magnetotelluric images of the crust and mantle in the southwestern Taurides, Turkey, *Tectonophysics,* **391**(1–4), 109–120, doi:10.1016/j.tecto.2004.07.012.

Gurrola, H., Minster, J.B. & Owens, T., 1994. The use of velocity spectrum for stacking receiver functions and imaging upper mantle discontinuities, *Geophys. J. Int.,* **117,** 427–440.

Helffrich, G., 2006. Extended-time multitaper frequency domain cross-correlation receiver-function estimation, *Bull. seism. Soc. Am.,* **96**(1), 344–347.

İlkışık, O.M., 1995. Regional heat flow in western Anatolia using silica temperature estimates from thermal springs, *Tectonophysics,* **244**(1–3), 175–184, doi:10.1016/0040-1951(94)00226-Y.

Jackson, J., 1994. Active tectonics of the Aegean region, *Ann. Rev. Earth planet. Sci.,* **22,** 239–271.

Kalyoncuoğlu, Ü.Y., Elitok, Ö., Dolmaz, M.N. & Anadolu, N.C., 2011. Geophysical and geological imprints of southern Neotethyan subduction between Cyprus and the Isparta Angle, SW Turkey, *J. Geodyn.,* **52**(1), 70–82, doi:10.1016/j.jog.2010.12.001.

Karabulut, H., Özalaybey, S., Taymaz, T., Aktar, M., Selvi, O. & Kocaoğlu, A., 2003. A tomographic image of the shallow crustal structure in the Eastern Marmara, *Geophys. Res. Lett.—AGU,* **30**(24), 2277–2280, December 2003, doi:10.1029/2003GL018074.

Kennett, B.L.N. & Engdahl, E.R., 1991. Travel times for global earthquake location and phase identification, *Geophys. J. Int.,* **105,** 429–465.

Keskin, M., 2003. Magma generation by slab steepening and breakoff beneath a subduction–accretion complex: an alternative model for collision-related volcanism in Eastern Anatolia, Turkey, *Geophys. Res. Lett.,* **30**(24), 8046, doi:10.1029/2003GL018019.

Keskin, M., Genç, Ş.C. & Tüysüz, O., 2008. Petrology and geochemistry of post-collisional Middle Eocene volcanic units in North-Central Turkey: evidence for magma generation by slab breakoff following the closure of the Northern Neotethys Ocean, *Lithos,* **104**(1–4), 267–305, doi:10.1016/j.lithos.2007.12.011.

Koulakov, I. & Sobolev, S.V., 2006. Moho depth and three-dimensional P and S structure of the crust and uppermost mantle in the Eastern Mediterranean and Middle East derived from tomographic inversion of local ISC data, *Geophys. J. Int.,* **164,** 218–235, doi:10.1111/j.1365-246X.2005.02791.x.

Lei, J. & Zhao, D., 2007. Teleseismic evidence for a break-off subducting slab under Eastern Turkey, *Earth planet. Sci. Lett.,* **257**(1–2), 14–28.

Ligorria, J.P. & Ammon, C.J., 1999. Iterative deconvolution and receiver-function estimation, *Bull. seism. Soc. Am.,* **89**(5), 1395–1400.

McClusky, S. *et al.*, 2000. Global Positioning System constraints on plate kinematics and dynamics in the eastern Mediterranean and Caucasus, *J. geophys. Res.,* **105**(B3), 5695–5720, doi:10.1029/1999JB900351.

McKenzie, D., 1978. Active tectonics of the Alpine-Himalayan Belt: the Aegean sea and surrounding regions, *Geophys. J. R. astr. Soc.,* **55,** 217–254.

Niu, F. & James, D.E., 2002. Fine structure of the lowermost crust beneath the Kaapvaal craton and its implications for crustal formation and evolution, *Earth planet. Sci. Lett.,* **200**(1–2), 121–130, doi:10.1016/S0012-821X(02)00584-8.

Okay, A.İ. & Satır, M., 2006. Geochronology of Eocene plutonism and metamorphism in northeast Turkey: evidence for a possible magmatic arc, *Geodinamica Acta*, **19**(5), 251–266.

Owens, T.J., Zandt, G. & Taylor, S.R., 1984. Seismic evidence for an ancient rift beneath the Cumberland plateau, Tennessee: a detailed analysis of broadband teleseismic P waveforms, *J. geophys. Res.,* **89,** 7783–7795.

Özacar, A.A., Zandt, G., Gilbert, H. & Beck, S.L., 2010. In Sedimentary Basin Tectonics from the Black Sea and Caucasus to the Arabian Platform, Seismic images of crustal variations beneath the East Anatolian Plateau (Turkey) from teleseismic receiver functions, Vol. 340, pp. 485–496, eds Sosson, M., Kaymakci, N., Stephenson, R.A., Bergerat, F. & Starostenko, V., Geological Society, London, Special Publications.

Park, J. & Levin, V., 2000. Receiver functions from multiple-taper spectral correlation estimates, *Bull. seism. Soc. Am.,* **90,** 1507–1520.

Pasquarè, G., Poli, S., Vezzoli, L. & Zanchi, A., 1988. Continental arc volcanism and tectonic setting in Central Anatolia, Turkey, *Tectonophysics,* **146,** 217–230.

Poppeliers, C. & Pavlis, G., 2003. Three-dimensional, prestack, plane wave migration of teleseismic P-to-S converted phases: 1. Theory, *J. geophys. Res.,* **108**(B2), 2112, doi:10.1029/2001JB000216.

Peng, X. & Humphreys, E.D., 1997. Moho dip and crustal anisotropy in Northwestern Nevada from teleseismic receiver functions, *Bull. seism. Soc. Am.,* **87,** 745–754.

Salah, M.K., Sahin, S. & Aydin, U., 2011. Seismic velocity and Poisson's ratio tomography of the crust beneath East Anatolia, *J. Asian Earth Sci.,* **40**(3), 746–761, doi:10.1016/j.jseaes.2010.10.021.

Savage, M.K, 1998. Lower crustal anisotropy or dipping boundaries? Effects on receiver functions and a case study in New Zealand, *J. geophys. Res.,* **103**(B7), 15 069–15 087.

Saunders, P., Priestly, K. & Taymaz, T., 1998. Variations in the crustal structure benath Western Turkey, *J. geophys. Int.,* **13,** 373–389.

Şengör, A.M.C & Yilmaz, Y., 1981. Tethyan evolution of Turkey: a plate tectonic approach, *Tectonophysics*, **75**(3–4), 181–190, 193–199, 203–241, doi:10.1016/0040-1951(81)90275-4.

Şengör, A.M.C., Özeren, S., Genç, T. & Zor, E., 2003. East Anatolian high plateau as a mantle-supported, north-south shortened domal structure, *Geophys. Res. Lett.,* **30**(24), 8045, doi:10.1029/2003GL017858.

Şengör, A.M.C., Tüysüz, O., Imren, C., Sakınç, M., Eyidogan, H., Görür, N., Le Pichon, X. & Rangin, C., 2005. The North Anatolian Fault: a new look, *Ann. Rev. Earth planet. Sci.,* **33,** 37–112.

Smith, W.H.F. & Wessel, P., 1990. Gridding with continuous curvature splines in tension, *Geophysics,* **55,** 293–305.

Tan, O. & Taymaz, T., 2006. Active tectonics of the Caucasus: earthquake source mechanisms and rupture histories obtained from inversion of teleseismic body-waveforms, in *Post-Collisional Tectonics and Magmatism in the Mediterranean Region and Asia,* pp. 531–578, Geological Society of America, Special Paper 409, doi:10.1130/2006.2409(25).

Taymaz, T., Jackson, J. & Mckenzie, D.P., 1991a. Active tectonics of the North and Central Aegean Sea, *Geophys. J. Int.,* **106,** 433–490.

Taymaz, T., Eyidogan, H. & Jackson, J.A., 1991b. Source Parameters of large earthquakes in the East Anatolian Fault Zone (Turkey), *Geophys. J. Int.,* **106,** 537–550.

Taymaz, T. & Price, S., 1992. The 1971 May 12 Burdur earthquake sequence, SW Turkey: a synthesis of seismological and geological observations, *Geophys. J. Int.,* **108,** 589–603.

Taymaz, T., 1993. The source parameters of Çubukdağ (Western Turkey) earthquake of 11 October 1986, *Geophys. J. Int.,* **108,** 589–603.

Taymaz, T., 1996. S-P wave travel-time residuals from earthquakes and lateral inhomogeneity in the upper mantle beneath the Aegean and the Hellenic trench near Crete, *Geophys. J. Int.,* **127,** 545–558.

Taymaz, T., Westaway, R. & Reilinger, R., 2004. Active faulting and crustal deformation in the Eastern Mediterranean Region, *Tectonophysics,* **391**(1–4), 375, doi:10.1016/j.tecto.2004.07.005.

Taymaz, T., Yılmaz, Y. & Dilek, Y., 2007a. Introduction, in *The Geodynamics of the Aegean and Anatolia,* Vol. 291, pp. 1–16, Geol. Soc. Spec. Pub. London, ISBN:978–1-86239–239-7, December 2007.

Taymaz, T., Wright, T., Yolsal, S., Tan, O., Fielding, E. & Seyitoğlu, G. 2007b. Source characteristics of June 6, 2000 Orta-Çankırı (Central Turkey) Earthquake: a synthesis of seismological, geological and geodetic (InSAR) observations, and internal deformation of Anatolian plate, in *The Geodynamics of the Aegean and Anatolia,* Vol. 291, pp. 259–290, The Geological Society of London, Special Publications, ISBN: 978–1-86239–239-7, December 2007.

Vinnik, L.P., Aleshin, I.M., Kiselev, S.G., Kosarev, G.L. & Makeyeva, L.I., 2007. Depth localized azimuthal anisotropy from SKS and P receiver functions: the Tien Shan, *Geophys. J. Int.,* **169**(3), 1289–1299, doi:10.1111/j.1365-246X.2007.03394.x.

Yilmaz, Y., 1990. Comparison of young volcanic associations of western and eastern Anatolia formed under a compressional regime: a review, *J. Volcanol. Geotherm. Res.,* **44,** 69–87.

Yolsal-Çevikbilen, S., Biryol, C., Beck, S., Zandt, G., Taymaz, T., Adiyaman, H. & Özacar, A., 2012. 3-D Crustal structure along the North Anatolian Fault Zone in North Central Anatolia revealed by local earthquake tomography, *Geophys. J. Int.,* **188,** 819–849, doi:10.1111/j.1365-246X.2011.05313.x.

Yolsal-Çevikbilen, S. & Taymaz, T., 2012. Earthquake source parameters along the Hellenic Subduction Zone and numerical simulations of historical tsunamis in the Eastern Mediterranean, *Tectonophysics,* **536–537,** 61–100, doi:10.1016/j.tecto.2012.02.019.

Zhu, L. & Kanamori, H., 2000. Moho depth variation in southern California from teleseismic receiver functions, *J. geophys. Res.,* **105,** 2969–2980.

Zor, E., Sandvol, E., Gürbüz, C., Türkelli, N., Seber, D. & Barazangi, M., 2003. The crustal structure of the East Anatolian plateau (Turkey) from receiver functions, *Geophys. Res. Lett.,* **30**(24), 8044, doi:10.1029/2003GL018192.

SUPPORTING INFORMATION

Additional Supporting Information may be found in the online version of this article:

Figure S1. Data plotted for the station, KO_BCK, located at 37.46°E, 30.59°N. The three left-hand panels are the backazimuth sweeps. The lower right panels are the epicentral distance sweeps. The upper right panels are the two H–K stacks with a weighting of 0.5 on the *P*s and 0.5 on the 2p1s (labelled 100/0) or a weighting of 0.5 on the *P*s, 0.25 on the 2p1s, and 0.25 on the 1p2s phases (labelled 50/50).

Figure S2. Same as Fig. S1, but data for the station KO_GADA located at 40.19°E, 25.90°N.

Figure S3. Same as Fig. S1, but data for the station KO_ISP located at 37.82°E, 30.52°N.

Figure S4. Same as Fig. S1, but data for the station TU_BOZC (ERD_BOZC) located at 39.84°E, 26.05°N.

Figure S5. Same as Fig. S1, but data for the station TU_HCB (DAF_HCB) located at 37.34°E, 36.91°N.

Figure S6. Same as Fig. S1, but data for the station TU_URLA (ERD_URLA) located at 40.19°E, 25.90°N.

Table S1. Receiver function H–K stacking results for the data in this study. The 50/50 H–K method refers to data stacked with the following weighting: 0.5 on the *P*s, 0.25 one the 2p1s, 0.25 on the 1p2s. The 100/0 H–K Moho depth refers to stacking using a weighting of 0.5 on the *P*s, 0.5 one the 2p1s, and 0.0 on the 1p2s. Data with apparent slab interference, anisotropy, or other structural interference are marked with a *, *** and ** respectively. Note that the YL array is deconvolved with a higher water level with a value of 0.2. The ERD, MAR, DAF and EGE network abbreviations are components of the TU array in the context of this paper. The transverse to radial amplitude ratio is the calculated for the average for the *P* arrival and given as an absolute value, a high ratio is indicative of the presence of a dipping layer or complex crustal structure. (http://gji.oxfordjournals.org//lookup/supp1/doi:10.1093/gji/ggs107/-/DC1)

Please note: Oxford University Press are not responsible for the content or functionality of any supporting materials supplied by the authors. Any queries (other than missing material) should be directed to the corresponding author for the article.